12-2013

Time Dependent Density-Functional Theory - Linear Response

Bryan Edman Sundahl
University of Tennessee - Knoxville, bsundahl@utk.edu

To the Graduate Council:

I am submitting herewith a thesis written by Bryan Edman Sundahl entitled "Time Dependent Density-Functional Theory - Linear Response." I have examined the final electronic copy of this thesis for form and content and recommend that it be accepted in partial fulfillment of the requirements for the degree of Master of Science, with a major in Chemistry.

Jon P. Camden, Major Professor

We have read this thesis and recommend its acceptance:

Charles Feigerle, Robert J. Hinde

Accepted for the Council:
Carolyn R. Hodges

Vice Provost and Dean of the Graduate School

(Original signatures are on file with official student records.)

12-2013

Time Dependent Density-Functional Theory - Linear Response

Bryan Edman Sundahl
bsundahl@utk.edu

To the Graduate Council:

I am submitting herewith a thesis written by Bryan Edman Sundahl entitled "Time Dependent Density-Functional Theory - Linear Response." I have examined the final electronic copy of this thesis for form and content and recommend that it be accepted in partial fulfillment of the requirements for the degree of Master of Science, with a major in Chemistry.

Jon P. Camden, Major Professor

We have read this thesis and recommend its acceptance:

Charles Feigerle, Robert J. Hinde

Accepted for the Council:
Carolyn R. Hodges

Vice Provost and Dean of the Graduate School

(Original signatures are on file with official student records.)

Time Dependent Density-Functional Theory - Linear Response

A Thesis Presented for the

Master of Science

Degree

The University of Tennessee, Knoxville

Bryan Edman Sundahl

December 2013

Acknowledgements

I would like to express a sincere thanks to Prof. Robert Harrison for his knowledgable guidance, patient explanations of the questions posed by a wandering and curious mind and for his support during my tenure in graduate school at the University of Tennessee.

I would like to thank both Dr. Scott Thornton and Dr. Matt Reuter for their insights into all the unforeseen problems that come from scientific computation.

I would like to thank Dr. Nick Vence for his enduring positivity and software suggestions. I would like to thank Dr. Jacob Fosse-Tande for his willingness to help find and fix mistakes, none of which he created. I would like to thank Tara Michaels-Clark and Deborah Penchoff for inspirational conversations that would take the edge of frustration away from debugging seemingly endless lines of code.

I would like to thank Prof. Camden for serving as a my thesis committee chair, and both Dr. Robert Hinde and Dr. Chuck Feigerle for serving on my thesis committee.

Abstract

The formal derivation of the linear response of time-dependent density-functional theory as shown by E. K. U. Gross is presented. The transformation of formal theory to the working linear response equations in the form of Casida's eigenvalue equation is demonstrated, and the results are applied to small monatomic, diatomic and triatomic systems. The application of different operators to the perturbed density is discussed, with the most attention being given to the dynamic polarizabilities. The dynamic polarizabilities and excitation spectra for N_2 [nitrogen gas] are then analyzed. The first excitation energy is noted to be in line with Koopmans' theorem. Finally three orbital localization algorithms and their implementation are detailed, with comparisons between the one-sided and two-sided Jacobi implementations present. The performance of a serial and then a parallel algorithm are shown. The poor performance of parallel algorithm is explained.

Table of Contents

List of Tables

List of Figures

Introduction

The overarching theme of this document is evident as the basics of linear response under the umbrella of time-dependent density-functional theory. However, this work is simply the beginning, not the end. The machinery of linear response developed here is the necessary link between current work and the desired goal of calculating forces on excited states. Forces of the excited states will allow access to the calculation of the excited state geometries as well as measurable properties of these excited states. These lofty goals require a firm grounding, and since this grounding is in time-dependent density-functional theory, that is where attention was initially focused.

By its very nature, the time-independent Schrödinger equation is not analytically solvable for molecular systems due to many-body effects such as electron-electron correlation. This led to the development of numerous approximations in order to solve the Schrödinger equation, including Hartree-Fock [1] theory and Density-Functional theory [2]. Hartree-Fock theory reduces the many-body problem into a single-body problem in which a particle interacts with an averaged field that is created by the remaining particles. However Hartree-Fock theory does not include electron correlation by construction, which leads to poor results for strongly correlated systems. Electron correlation is the long range interaction in which every electron instantaneously feels the exact potential from every other electron present in the system, which will be different from the mean field experienced in Hartree-Fock. Extensions to Hartree-Fock theory have been made to include aspects missed in the original theory, including Møller-Plesset perturbation theory [3] or configuration

interaction methods [4] or, if your system is small enough, coupled cluster methods [5].

Density-Functional theory (DFT) takes a different approach to electronic structure. DFT focuses on the electronic density as the fundamental quantity as opposed to the wavefunction. By focusing on the density, DFT reduces the $4n$ degrees of freedom (three spatial variables and a spin variable) of an n electron system to the four degrees of freedom needed to specify the spin-density [6]. DFT also explicitly includes electron-electron correlation through its use of the exchange-correlation potential. The exchange-correlation potential is a mysterious and unknown functional of the electronic density that, if known exactly, would allow for exact results to be obtained through the use of DFT. DFT relies on the two Hohenberg-Kohn theorems [2] and the Kohn-Sham formula to arrive at a working set of equations.

DFT is strictly for ground state properties. In order to extend DFT to an excited state, the time-dependent Schrödinger equation must be solved. Doing so using DFT will yield the time-dependent density-functional theory equations (TD-DFT). TD-DFT has its own version of the Hohenberg-Kohn theorems that rigorously prove its validity. These theorems are detailed in subsequent chapters, and their implementation in another. The results are detailed and discussed in yet another chapter.

The final chapter explores the separate but related issue of orbital localization and the parallelization of the localization algorithms. SCF methods generate delocalized molecular orbitals that can be spread over an entire molecule, which is a non-physical distribution. Physically molecular orbitals are atom centered, and spatially spanning only a small number of near neighbor atomic centers. To turn a delocalized orbital spread throughout the molecule into an atom centered, spatially concentrated and hence physically relevant molecular orbital an orbital localization algorithm must be used. The common localization algorithms are discussed, along with their implementation. The implementation is derived from the Jacobi plane rotation eigenvalue algorithm, which is also discussed. The creation of a parallel code is then

explored, with communication patterns among processors and the difficulties therein commanding most of the attention.

Chapter 1

Time Dependent Density-Functional Theory

Time-dependent density functional theory is a many-body approach to evolve a wavefunction in time based only on the electronic particle density. There are two main components to the theory: the first is the Runge-Gross Theorem [7], which establishes for a fixed initial state a one-to-one mapping between the density and the external potential. A large consequence of this is that physical observables can be written as functionals of this density [8]. The second component is the Kohn-Sham formalism that is also present in the ground state theory. The Kohn-Sham formalism states that the density of an interacting system of electrons can be found from a similar but non-interacting system in which the particles interact only with an effective local multiplicative single-particle potential.

1.1 The Runge-Gross Theorem

Time-dependent density functional theory is directly related to the time-dependent Schrödinger equation

$$i\frac{\partial}{\partial t}\Psi(t) = \hat{H}(t)\Psi(t) \tag{1.1}$$

where $\Psi(t)$ has an fixed, arbitrary initial condition $\Psi(t_0) = \Psi_0$. The Hamiltonian is known to be

$$\hat{H}(t) = \hat{T} + \hat{V}_{ee}(t) + \hat{V}_{ext}(t). \tag{1.2}$$

These operators describe the interactions of electrons. The operator $\hat{T}$ is simply the kinetic energy operator

$$\hat{T} = \sum_{j=1}^{N} -\frac{\nabla_j^2}{2}. \tag{1.3}$$

The operator $\hat{V}_{ee}$ is the Coulomb operator

$$\hat{V}_{ee}(t) = \frac{1}{2} \sum_{i \neq j}^{N} \frac{1}{|\mathbf{r}_i - \mathbf{r}_j|}. \tag{1.4}$$

The $\hat{V}_{ext}$ operator is the external potential operator and for this discussion will always be of the form

$$\hat{V}_{ext}(t) = \sum_{i=1}^{N} v(\mathbf{r}_i, t). \tag{1.5}$$

The functions $\hat{V}_{ext}(t)$ will be assumed to be Taylor expandable around initial time t_0. If the external potential is thus constructed then the theorem of Runge and Gross [7] is applicable:

Two solutions $\Psi(t)$ and $\Psi'(t)$ of the Schrödinger equation which evolve from a fixed common initial state Ψ_0 under the influence of the potentials $v(\mathbf{r}, t)$ and $v'(\mathbf{r}, t)$, respectively, always lead to different electron densities $\rho(\mathbf{r}, t)$ and $\rho'(\mathbf{r}, t)$, provided the two potentials $v(\mathbf{r}, t)$ and $v'(\mathbf{r}, t)$ differ by more than a purely time-dependent function, i.e.

$$v'(\mathbf{r}, t) \neq v(\mathbf{r}, t) + c(t) \tag{1.6}$$

The proof of this theorem is accomplished in two steps. The first step demonstrates a one-to-one correspondence between an external potential and a current density while the second step demonstrates a one-to-one correspondence between a current density

and an electronic density. *Modus ponens* then produces the desired result of a one-to-one correspondence between an external potential and an electronic density.

The first step is accomplished by considering the two potentials defined above, $v(\mathbf{r},t)$ and $v'(\mathbf{r},t)$, which differ by more than a time-dependent function [9]. Because both of these potentials can be expanded in a Taylor series about t_0, there exists some non-negative integer k such that

$$\frac{\partial^k}{\partial t^k}\left[v(\mathbf{r},t)-v'(\mathbf{r},t)\right]\Big|_{t=t_0} \neq constant. \tag{1.7}$$

Now consider the current densities arising from each potential. The current density $\mathbf{j}(\mathbf{r},t)$ is given by

$$\mathbf{j}(\mathbf{r},t) = N\int d^3r_2 \ldots \int d^3\, r_N \mathrm{Im}(\Psi(\mathbf{r},\mathbf{r_2},\ldots,\mathbf{r_N},t)\nabla\Psi^*(\mathbf{r},\mathbf{r_2},\ldots,\mathbf{r_N},t)). \tag{1.8}$$

The system corresponding to each potential differs from the other only in their single-body potential, and hence the equation of motion for the difference of the two current densities is

$$\begin{aligned}\frac{\partial}{\partial t}\left\{\mathbf{j}(\mathbf{r},t)-\mathbf{j}'(\mathbf{r},t)\right\}_{t=0} &= -\mathbf{i}\left\langle\Psi_0\left|\left[\hat{\mathbf{j}}(\mathbf{r},t),\left\{\hat{H}(0)-\hat{H}'(0)\right\}\right]\right|\Psi_0\right\rangle \\ &= -\mathbf{i}\left\langle\Psi_0\left|\left[\hat{\mathbf{j}}(\mathbf{r},t),\left\{v(\mathbf{r},0)-v'(\mathbf{r},0)\right\}\right]\right|\Psi_0\right\rangle \\ &= -n(\mathbf{r},0)\nabla\left\{v(\mathbf{r},0)-v'(\mathbf{r},0)\right\}\end{aligned} \tag{1.9}$$

where $n(\mathbf{r},0)$ is the initial electronic density. Thus it is shown that if at time t_0 the potentials differ by more than just a constant, then the first derivative of each of the currents must differ. This will cause the currents to differ at some time $t > t_0$. A similar approach to all subsequent derivatives is possible, yielding the following relation

$$\frac{\partial^{k+1}}{\partial t^{k+1}}\left\{\mathbf{j}\,(\mathbf{r},t)-\mathbf{j}'(\mathbf{r},t)\right\}_{t=0} = -n(\mathbf{r},0)\nabla\frac{\partial^k}{\partial t^k}\left\{v(\mathbf{r},t)-v'(\mathbf{r},t)\right\}_{t=0}. \tag{1.10}$$

Since equation (1.7) is valid and the potentials are both able to be Taylor expanded about t_0, then there exists a positive integer k such that the right hand side of (1.9) does not equal zero, i.e.

$$\mathbf{j}(\mathbf{r},t) \neq \mathbf{j}'(\mathbf{r},t). \tag{1.11}$$

The above establishes a one-to-one correspondence between potentials and current densities. The final step is to show the one-to-one correspondence between current densities and electronic densities. To make this connection, take the gradient of equation (1.10), along with the continuity of the Schrödinger equation, which gives

$$\frac{\partial^{k+2}}{\partial t^{k+2}}\{n\left(\mathbf{r},t\right) - n'(\mathbf{r},t)\}_{t=0} = \nabla \cdot \left[-n(\mathbf{r},0)\nabla \frac{\partial^k}{\partial t^k}\left\{v(\mathbf{r},t) - v'(\mathbf{r},t)\right\}_{t=0}\right]. \tag{1.12}$$

The last step is to prove the right hand side of (1.12) is non-zero for some k, which would mean that the density difference is non-zero. The proof is accomplished through contradiction. Let $f(\mathbf{r}) = \frac{\partial^k}{\partial t^k}\{v_{ext}(\mathbf{r},t) - v'_{ext}(\mathbf{r},t)\}|_{t=0}$. Now consider

$$\int d^3r\ f(\mathbf{r})\nabla \cdot [n_0(\mathbf{r})\nabla f(\mathbf{r})] = \int d^3r \left\{\nabla \cdot [f(\mathbf{r})n_0(\mathbf{r})\nabla f(\mathbf{r})] - n_0(\mathbf{r})\left|\nabla f(\mathbf{r})\right|^2\right\}. \tag{1.13}$$

The first term on the right hand side is recognizable as a surface integral at $r = \infty$. This surface integral decays rapidly enough for realistic potentials, that is at least as fast as $-1/r$, such that it can be concluded that the integral vanishes. The second term in equation (1.13) will be less than zero, which causes the left hand side of to be non-zero somewhere. If $\nabla f(\mathbf{r})$ is non-zero somewhere, then it is impossible for $\nabla(n_0\nabla f(\mathbf{r})$ to vanish everywhere. Therefor the densities $n(\mathbf{r},t)$ and $n'(\mathbf{r},t)$ differ in at least one term in their Taylor series, and as such differ by more than a time dependent phase factor. This completes the proof.

The wavefunction can be written as a functional of the density, which means

$$\Psi(t) = e^{-i\alpha(t)}\tilde{\Psi}\left[\rho\right](t) \tag{1.14}$$

and that observables will take the form

$$O\left[\rho\right]\left(t\right)=\left\langle \tilde{\Psi}\left[\rho\right]\left(t\right)\left|\hat{O}(t)\right|\tilde{\Psi}\left[\rho\right]\left(t\right)\right\rangle \tag{1.15}$$

taking note that the phase factor cancels.

1.2 The Time-Dependent Kohn-Sham Equation

The Runge-Gross theorem is valid for an *arbitrary* time-dependent potential, even for the potential $\hat{V}(t)=0$. This allows for the comparison between the physical, interacting system and the fictitious non-interacting system of particles with equal time-dependent densities. That is, consider a system with interacting particles and a time dependent density $\rho(\mathbf{r},t)$ and a system with non-interacting particles but the same time dependent density $\rho(\mathbf{r},t)$. The one-to-one mapping between densities and potentials guarantees a unique local effective potential $v_{KS}[\rho](\mathbf{r},t)$ for the non-interacting system which generates the same density as the interacting system. The existence of this v-representable potential was not included in the Runge and Gross paper, but was later proved by van Leeuwen [8].

The time-dependent KS equation, as defined in [9], has the form

$$i\frac{\partial\varphi_{j}(\mathbf{r},t)}{\partial t}=\left[-\frac{\nabla^{2}}{2}+v_{\mathrm{KS}}[n](\mathbf{r},t)\right]\varphi_{j}(\mathbf{r},t) \tag{1.16}$$

where $n(\mathbf{r},t)$ is the density of both the fictitious system and and the physical system and is

$$n(\mathbf{r},t)=\sum_{j=1}^{N}\left|\varphi_{j}(\mathbf{r},t)\right|^{2}. \tag{1.17}$$

Because of the proof above, the potential $v_{\mathrm{KS}}(\mathbf{r},t)$ is uniquely determined from this density. It can then be defined as

$$v_{\mathrm{KS}}=v_{\mathrm{ext}}(\mathbf{r},t)+v_{\mathrm{H}}(\mathbf{r},t)+f_{\mathrm{xc}}(\mathbf{r},t). \tag{1.18}$$

Here $v_{\mathrm{H}}(\mathbf{r}, t)$ is the time-dependent Hartree potential

$$v_{\mathrm{H}}[\rho](\mathbf{r}, t) = \int \frac{\rho(\mathbf{r}', t)}{|\mathbf{r} - \mathbf{r}'|} \tag{1.19}$$

and $f_{\mathrm{xc}}(\mathbf{r}, t)$ is the exchange-correlation kernel. Just like the exchange-correlation potential in ground state DFT, the exchange-correlation kernel is unknown, and in the limit that it becomes exactly known, the TDDFT equation will yield exact results. Unlike the exchange-correlation potential in ground state DFT the exchange-correlation kernel is a function of the entire history of the density, along with both the initial wavefunction $\Psi(0)$ and the initial KS wavefunction $\Phi(0)$.

1.3 Linear Response Formalism

Even with the improved locality of the time-dependent density-functional theory over other theories such as time-dependent Hartree-Fock or configuration interaction, full solutions to the time-dependent Kohn-Sham equation can be expensive to calculate for even moderately sized systems. To alleviate this cost the linear response of the system can be taken as a first approximation to the full solution. Linear response also possesses the allure of producing exact excitation energies [10], in the limit of the exact exchange-correlation kernel. Properties that are formally the derivative of the energy with respect to a perturbation can be calculated within the framework of linear response theory. Calculating the linear response can be accomplished using perturbation theory. Following the work of [11], this can be shown as follows.

Consider a small perturbation $v_1(\mathbf{r}, t)$ turned on at time t_0. The system will respond to this perturbation, and the response can be written as a Taylor series

$$\rho(\mathbf{r}, t) - \rho_0(\mathbf{r}, t) = \rho_1(\mathbf{r}, t) + \rho_2(\mathbf{r}, t) + \rho_3(\mathbf{r}, t) + \cdots \tag{1.20}$$

where the subscripts indicate the order of the external perturbation and $\rho_0(\mathbf{r},t)$ is the ground-state density of the unperturbed system. Then the first order response can be written as

$$\rho_1(\mathbf{r},t) = \int\int \chi(\mathbf{r},t,\mathbf{r}',t)v_1(\mathbf{r}',t)d^3r'dt \tag{1.21}$$

where χ is the density response of the interacting system

$$\chi(\mathbf{r},t,\mathbf{r}',t') = \left.\frac{\delta\rho\left[v_{ext}\right](\mathbf{r},t)}{\delta v_{ext}(\mathbf{r}',t)}\right|_{v_0}. \tag{1.22}$$

Applying the chain rule for the functional gives

$$\chi(\mathbf{r},t,\mathbf{r}',t') = \int\int \frac{\delta\rho(\mathbf{r},t)}{\delta v_{\mathrm{KS}}(\mathbf{y},\tau)}\left.\frac{\delta v_{\mathrm{KS}}(\mathbf{y},\tau)}{\delta v_{ext}(\mathbf{r}',t')}\right|_{v_0} d^3y d\tau. \tag{1.23}$$

Next, take the functional derivative of equation (1.18) with respect to the external potential

$$\frac{\delta v_{\mathrm{KS}}(\mathbf{r},t)}{\delta v_{ext}(\mathbf{r}',t')} = \delta(\mathbf{r}-\mathbf{r}')\delta(t-t') + \int\int\left(\frac{\delta(t-\tau)}{|\mathbf{r}-\mathbf{y}|} + \frac{\delta v_{xc}(\mathbf{r},t)}{\delta\rho(\mathbf{y},\tau)}\right)\frac{\delta\rho(\mathbf{y},\tau)}{\delta v_{ext}(\mathbf{r}',t')}d^3y d\tau. \tag{1.24}$$

Inserting equation (1.24) into equation (1.23) gives

$$\begin{aligned}\chi(\mathbf{r},t,\mathbf{r}',t') = \chi_{\mathrm{KS}}(\mathbf{r},t,\mathbf{r}',t') + \int d^3y\int d\tau\int d^3y'\int d\tau'\chi_{\mathrm{KS}}(\mathbf{r},t,\mathbf{r}',t') \\ \times\left(\frac{\delta(\tau-\tau')}{|\mathbf{y}-\mathbf{y}'|} + f_{xc}[\rho_0](\mathbf{y},\tau,\mathbf{y}',\tau')\right)\chi(\mathbf{y}',\tau',\mathbf{r}',t')\end{aligned} \tag{1.25}$$

where $\chi_{\mathrm{KS}}(\mathbf{r},t,\mathbf{r}',t)$ is the Kohn-Sham response function

$$\chi_{\mathrm{KS}}(\mathbf{r},t,\mathbf{r}',t) := \left.\frac{\delta\rho[v_{\mathrm{KS}}](\mathbf{r},t)}{\delta v_{\mathrm{KS}}(\mathbf{r}',t')}\right|_{v_{\mathrm{KS}}[\rho_0]} \tag{1.26}$$

and $f_{xc}[\rho_0](\mathbf{r},t,\mathbf{r}',t')$ is the exchange-correlation kernal

$$f_{xc}[\rho_0](\mathbf{r},t,\mathbf{r}',t') := \left.\frac{\delta v_{xc}[\rho](\mathbf{r},t)}{\delta\rho(\mathbf{r}',t')}\right|_{\rho_0}. \tag{1.27}$$

Equation (1.25) is the key equation in time-dependent density-functional theory, as it relates the fictitious non-interacting system to the physically relevant interacting system. If you insert equation (1.25) into equation (1.21) then the linear response of the density can be equated as

$$\rho_1(\mathbf{r},t) = \int\int \chi_{\mathrm{KS}}(\mathbf{r},t,\mathbf{r}',t])v_{\mathrm{KS},1}(\mathbf{r}',t)d^3r'dt' \tag{1.28}$$

where the effective potential

$$v_{\mathrm{KS},1}(\mathbf{r}',t) = v_1(\mathbf{r},t) + \int \frac{\rho_1(\mathbf{r}',t)}{|\mathbf{r}-\mathbf{r}'|}d^3r' + \int\int f_{xc}[\rho_0](\mathbf{r},t,\mathbf{r}',t')\rho_1(\mathbf{r};,t)d^3r'dt' \tag{1.29}$$

holds the external perturbation $v_1(\mathbf{r},t)$, the Hartree Coulomb potential and the unknown exchange-correlation potential.

To this point all work has been done in real-space. It is advantageous to consider the same equations in frequency space, especially for calculating properties such as polarizabilities or excitation energies. To transition into frequency space, a Fourier transform of equations (1.28) and (1.29) must be performed, yielding the frequency-dependent linear response equation

$$\begin{aligned}\rho_1(\mathbf{r},\omega) = &\int \chi_{\mathrm{KS}}(\mathbf{r},\mathbf{y};\omega)v_1(\mathbf{y},\omega)d^3y \\ &+ \int\int \chi_{\mathrm{KS}}(\mathbf{r},\mathbf{y};\omega)\left(\frac{1}{|\mathbf{y}-\mathbf{y}'|} + f_{xc}[\rho_0](\mathbf{y},\mathbf{y}';\omega)\right)\rho_1(\mathbf{y}',\omega)d^3y\ d^3y'.\end{aligned} \tag{1.30}$$

The frequency-dependent Kohn-Sham response function χ_{KS} can also be expressed in terms of its sum over states form, which is

$$\chi_{\mathrm{KS}}(\mathbf{r},\mathbf{r}';\omega) = \sum_{j,k}(f_k - f_j)\frac{\psi_j(\mathbf{r})\psi_k^*(\mathbf{r})\psi_k^*(\mathbf{r})\psi_j(\mathbf{r}')}{\omega - (\epsilon_j - \epsilon_k) + i\eta} \tag{1.31}$$

where f_k is the occupation number of groundstate Kohn-Sham orbital $\psi_k(\mathbf{r})$ with orbital energy ϵ_k. Inspection of the sum over states formula shows that as $\omega \to (\epsilon_j - \epsilon_k)$ (i.e. the exact excitation energy) the right hand side will approach a pole.

1.4 Matrix Formulation of the Response Equations

Following the work of Casida [12] equation (1.31) can be transformed into a matrix representation. To see this, expand equation (1.31) as

$$\begin{aligned}
\chi_{\mathrm{KS}}(\mathbf{r},\mathbf{r}';\omega) &= \sum_{j,k}(f_k - f_j)\frac{\psi_j(\mathbf{r})\psi_k(\mathbf{r}')\psi_k^*(\mathbf{r})\psi_j^*(\mathbf{r}')}{\omega - (\epsilon_j - \epsilon_k) + i\eta} \\
&= \sum_{k=1}^{N}\sum_{j=1}^{\infty}\frac{\psi_j(\mathbf{r})\psi_k(\mathbf{r}')\psi_k^*(\mathbf{r})\psi_j^*(\mathbf{r}')}{\omega - (\epsilon_j - \epsilon_k)} - \sum_{k=1}^{N}\sum_{j=1}^{\infty}\frac{\psi_k(\mathbf{r})\psi_j(\mathbf{r}')\psi_j^*(\mathbf{r})\psi_k^*(\mathbf{r}')}{\omega + (\epsilon_j - \epsilon_k)} \\
&= \sum_{i,a}\left(\frac{\psi_a(\mathbf{r})\psi_i(\mathbf{r}')\psi_i^*(\mathbf{r})\psi_a^*(\mathbf{r}')}{\omega - (\epsilon_a - \epsilon_i)} - \frac{\psi_i(\mathbf{r})\psi_a(\mathbf{r}')\psi_a^*(\mathbf{r})\psi_i(\mathbf{r}')}{\omega + (\epsilon_a - \epsilon_i)}\right)
\end{aligned} \tag{1.32}$$

where the subscript i takes values 1 through N, representing the occupied orbitals, and a takes values $N+1$ through ∞, representing the virtual orbitals of a complete basis set. Now let

$$P_{ai}(\omega) = \frac{\int \psi_i(\mathbf{r}')\psi_a^*(\mathbf{r}')v_{\mathrm{KS},1}(\mathbf{r}',\omega)d^3r'}{\omega - (\epsilon_a - \epsilon_i)} \tag{1.33}$$

and

$$P_{ia}(\omega) = \frac{\int \psi_a(\mathbf{r}')\psi_i^*(\mathbf{r}')v_{\mathrm{KS},1}(\mathbf{r}',\omega)d^3r'}{-(\omega + (\epsilon_a - \epsilon_i))} \tag{1.34}$$

then the linear density response can be shown to be

$$\rho_1(\mathbf{r},\omega) = \sum_{i,a} \psi_a(\mathbf{r})\psi_i^*(\mathbf{r})P_{ai}(\omega) + \psi_i(\mathbf{r})\psi_a^*(\mathbf{r})P_{ia}(\omega). \tag{1.35}$$

A small rearrangement of equations (1.33) and (1.34) gives

$$(\omega - (\epsilon_a - \epsilon_i))P_{ai}(\omega) = \int \psi_i(\mathbf{r}')\psi_a^*(\mathbf{r}')v_{\mathrm{KS},1}(\mathbf{r}',\omega)d^3r' \tag{1.36}$$

and

$$(\omega + (\epsilon_a - \epsilon_i))P_{ia}(\omega) = -\int \psi_a(\mathbf{r}')\psi_i^*(\mathbf{r}')v_{\mathrm{KS},1}(\mathbf{r}',\omega)d^3r'. \tag{1.37}$$

Letting the Hartree and exchange-correlation potentials be written as

$$f_{H_{xc}}(\mathbf{r},\mathbf{r}',\omega) = \frac{1}{|\mathbf{r}-\mathbf{r}'|} + f_{xc}(\mathbf{r},\mathbf{r}',\omega) \tag{1.38}$$

then matrix elements $v_{ai}(\omega)$ can be defined as

$$v_{ai}(\omega) := \int \psi_i(\mathbf{r})v_1(\mathbf{r},\omega)\psi_a^*(\mathbf{r})d^3r \tag{1.39}$$

and

$$K_{kl,mn}(\omega) = \int\int \psi_k(\mathbf{r})\psi_l^*(\mathbf{r})f_{H_{xc}}(\mathbf{r},\mathbf{r}',\omega)\psi_m(\mathbf{r}')\psi_n^*(\mathbf{r}')d^3rd^3r'. \tag{1.40}$$

These, along with equations (1.35) and (1.36) gives the matrix form of the frequency dependent linear response of the density as

$$(\omega - (\epsilon_a - \epsilon_i))P_{ai}(\omega) = v_{ai}(\omega) + \sum_{j,b}(P_{bj}(\omega)K_{ai,bj}(\omega) + P_{jb}(\omega)K_{ai,bj}(\omega)) \tag{1.41}$$

which is equivalent to

$$\sum_{j,b}\left\{\left[\delta_{ij}\delta_{ab}(\epsilon_a - \epsilon_i - \omega) + K_{ai,bj}(\omega)\right]P_{bj}(\omega) + K_{ai,bj}(\omega)P_{jb}(\omega)\right\} = -v_{ai}(\omega). \tag{1.42}$$

Using equation (1.37) instead of equation (1.36) will give

$$\sum_{j,b} \left\{ \left[\delta_{ij}\delta_{ab}(\epsilon_a - \epsilon_i + \omega) + K_{ai,jb}(\omega) \right] P_{jb}(\omega) + K_{ai,bj}(\omega) P_{bj}(\omega) \right\} = -v_{ia}(\omega). \quad (1.43)$$

Defining

$$X_{jb}(\omega) = P_{jb}(\omega) \quad (1.44)$$

$$Y_{jb}(\omega) = P_{bj}(\omega) \quad (1.45)$$

$$A_{ia,jb}(\omega) = \delta_{ij}\delta_{ab}(\epsilon_a - \epsilon_i) + K_{ai,jb}(\omega) \quad (1.46)$$

$$B_{ia,jb}(\omega) = K_{ia,bj}(\omega) \quad (1.47)$$

$$Q_{ia}(\omega) = -v_{ai}(\omega) \quad (1.48)$$

$$R_{ia}(\omega) = -v_{ia}(\omega) \quad (1.49)$$

allows the construction of a very compact notation of equations (1.42) and (1.43) in matrix form

$$\left[\begin{pmatrix} A(\omega) & B(\omega) \\ B^*(\omega) & A^*(\omega) \end{pmatrix} - \omega \begin{pmatrix} -1 & 0 \\ 0 & 1 \end{pmatrix} \right] \begin{pmatrix} X(\omega) \\ Y(\omega) \end{pmatrix} = \begin{pmatrix} Q(\omega) \\ R(\omega) \end{pmatrix}. \quad (1.50)$$

If the orbitals are real valued and fxc is independent of the incident frequency, then equation (1.50) can be turned into a pseudo-eigenvalue problem. To see this, first take the sum and difference respectively of each of the equations presented in (1.50). Doing so gives

$$(A + B)(Y + X)_q = \Omega_q (Y - X)_q \quad (1.51)$$

$$(A - B)(Y - X)_q = \Omega_q (Y + X)_q \quad (1.52)$$

where the q index indicates which eigenvector is being considered. Solving equation (1.52) for $(X - Y)_q$ and putting that into equation (1.51) gives

$$(A - B)(A + B)(X + Y)_q = \Omega_q^2 (X + Y)_q. \quad (1.53)$$

Since the matrix $(A-B)$ has only positive values on its diagonal it is positive definite which means (1.53) can be written as

$$(A-B)^{1/2}(A+B)(A-B)^{1/2}(A-B)^{-1/2}(X+Y)_q = \Omega_q^2(A-B)^{-1/2}(X+Y)_q \quad (1.54)$$

which is usually denoted as

$$WF_q = \Omega_q^2 F_q \quad (1.55)$$

where

$$F_q = (A-B)^{-1/2}(X+Y)_q \quad (1.56)$$

and

$$W = (A-B)^{1/2}(A+B)(A-B)^{1/2}. \quad (1.57)$$

As noted by Casida [12] the eigenvalues of W are going to be the squares of the excitation energies. The value of the matrix B in equation (1.50) gives rise to different approximations that all fit within this linear response framework. If $B = 0$, then the Tamm-Dancoff approximation [13] is being employed and the matrix equation reduces to the simpler Configuration-Interaction (singles) equation of

$$\mathbf{AX} = \omega\mathbf{X} \quad (1.58)$$

where $\mathbf{A}$ and $\mathbf{X}$ have the same definitions as above. If the potential $f_{H_{xc}}$ in (1.40) contains only an exchange term and no electron correlation, then these equations are better known as Random Phase Approximation (RPA) equations.

Chapter 2

Generality of Response Theory and Implementation

Response theory is limited to the calculation of properties that can be formally written as a derivative of the ground state energy with respect to a parameter λ [14]. Fortunately there are many forms of λ leading to many different interesting properties that may be calculated. The focus of this work is on the polarizability, and by extension the excitation energies, of molecules. Other well known properties such as NMR shielding tensors or magnetizabilities can also be derived from response theory.

2.1 Generality

Following the discussion of Autschbach and Ziegler [14], consider property B of a molecule. The expectation value is then written as

$$B_0 = \left\langle \Psi_0 \left| \hat{B} \right| \Psi_0 \right\rangle \tag{2.1}$$

where $\hat{B}$ is the expected notation of the operator for the observable B and subscripts of 0 refer to the ground state. The expectation value of $\langle B \rangle$ and the physical property

will share the same notation of B for simplicity. Note that because the physical properties are derivatives of the energy of the molecule with respect to an external perturbation λ what is actually being calculated is

$$B_0 = E_0^{(1)} = \left.\frac{\partial E_0}{\partial \lambda}\right|_{\lambda=0} = \left\langle \Psi_0 \left| \hat{H}^{(1)} \right| \Psi_0 \right\rangle . \tag{2.2}$$

This relation makes use of the Hellmann-Feynman theorem to remove the terms containing derivatives of the wavefunction [15]. Comparison of equation (2.1) with (2.2) gives the relation $\hat{B} = \hat{H}^{(1)}$. The properties of interest, such as the transition energies, are actually derivatives of B with respect to the perturbation. Differentiation of equation (2.2) with respect to the perturbation gives

$$\begin{aligned} B^{(1)} = \left.\frac{\partial B}{\partial \lambda}\right|_{\lambda=0} &= E^{(2)} = \left.\frac{\partial^2 E}{\partial \lambda^2}\right|_{\lambda=0} \\ &= \left\langle \Psi_0 \left| \hat{H}^{(1)} \right| \Psi_0^{(1)} \right\rangle + \left\langle \Psi_0^{(1)} \left| \hat{H}^{(1)} \right| \Psi_0 \right\rangle + \left\langle \Psi_0 \left| \hat{H}^{(2)} \right| \Psi_0 \right\rangle \\ &= \left\langle \Psi_0 \left| \hat{B} \right| \Psi_0^{(1)} \right\rangle + \left\langle \Psi_0^{(1)} \left| \hat{B} \right| \Psi_0 \right\rangle + \left\langle \Psi_0 \left| \hat{B}^{(1)} \right| \Psi_0 \right\rangle . \end{aligned} \tag{2.3}$$

Similarly if one wished to consider two different perturbations λ_1 and λ_2 simultaneously, then the energy in a "perturbative series expansion" as created in [16] is

$$E = E^{(0,0)} + E^{(1,0)}\lambda_1 + E^{(0,1)}\lambda_2 + E^{(1,1)}\lambda_1\lambda_2 + E^{(2,0)}\lambda_1^2 + \cdots . \tag{2.4}$$

Then differentiation of (2.4) with respect to both parameters gives

$$\begin{aligned} B^{(0,1)} = \left.\frac{\partial B}{\partial \lambda_2}\right|_{\lambda_2=0} &= E^{(1,1)} = \left.\frac{\partial^2 E}{\partial \lambda_1 \lambda_2}\right|_{\lambda_1=0,\lambda_2=0} \\ &= \left\langle \Psi_0^{(0,0)} \left| \hat{H}^{(1,0)} \right| \Psi_0^{(0,1)} \right\rangle + \left\langle \Psi_0^{(0,1)} \left| \hat{H}^{(1,0)} \right| \Psi_0^{(0,0)} \right\rangle + \left\langle \Psi_0^{(0,0)} \left| \hat{H}^{(1,1)} \right| \Psi_0^{(0,0)} \right\rangle \\ &= \left\langle \Psi_0^{(0,0)} \left| \hat{B}^{(0,0)} \right| \Psi_0^{(0,1)} \right\rangle + \left\langle \Psi_0^{(0,1)} \left| \hat{B}^{(0,0)} \right| \Psi_0^{(0,0)} \right\rangle + \left\langle \Psi_0^{(0,0)} \left| \hat{B}^{(0,1)} \right| \Psi_0^{(0,0)} \right\rangle \end{aligned} \tag{2.5}$$

It is this response property $B^{(1)}$ or $B^{(0,1)}$ that is the main point of interest. There are two classifications of response properties: static and dynamic. Dynamic response

properties are those that depend on a time-dependent perturbation. Static response properties are those that arise from time-independent perturbations. Static properties can be viewed as a limiting case of the dynamic response when the frequency of the perturbing potential is reduced to zero ($\omega \to 0$). For some applications, the term containing $B^{(0,1)}$ is negligibly small or even non-existent [14]. In cases where this is not applicable, such as when investigating the NMR shielding tensor, the term is easy to compute since it is only the expectation value of the known reference state wavefunction. The method for determining $B^{(1)}$ has been presented previously, with the ultimate equation being (1.50).

2.2 Static Properties

An examples of a static property is the nuclear magnetic resonance (NMR) shielding tensor. This can be seen by first considering the classical interaction between a nuclear magnetic moment and an external magnetic field $\mathbf{B}$ which is known to be

$$E = -\mu_A \cdot \mathbf{B} \tag{2.6}$$

where μ_A is the spin magnetic moment of the respective nucleus. Atoms and molecules in experiments exhibit different behavior as the electrons shield the nucleus from the full effects of the field $\mathbf{B}$, or more precisely

$$E = -\mu_A \cdot (1 - \sigma)\mathbf{B} \tag{2.7}$$

with σ representing the nuclear shielding tensor for nucleus A in the given chemical environment. This tensor is more formally defined as

$$\sigma_A = \left. \frac{\partial^2 E}{\partial \mathbf{B} \partial \mu_A} \right|_{\mathbf{B}=0, \mu_A=0} \tag{2.8}$$

which fits the form of (2.5), and thus can be calculated using Response Theory. As stated above, for this property the diamagnetic term $\left\langle \Psi_0^{(0,0)} \middle| \hat{B}^{(0,1)} \middle| \Psi_0^{(0,0)} \right\rangle$ is not negligible and must be explicitly included.

2.3 Dynamic Properties

A prime example of a dynamic response property is the polarizability, which relates the perturbation of a molecule's electron cloud by an applied external electric field $\mathbf{E}$. This relation is

$$D^{(1)} = \alpha \mathbf{E} \tag{2.9}$$

where α is the polarizability tensor and $D^{(1)}$ is the derivative of the molecular dipole with respect to the electric field $\mathbf{E}$. The dipole is itself the first-order energy change of a molecule in response to a perturbing electric field

$$D = \left. \frac{\partial E}{\partial \mathbf{E}} \right|_{\mathbf{E}=0}. \tag{2.10}$$

This means that the polarizability tensor α can be written as

$$\alpha = -\left. \frac{\partial^2 E}{\partial \mathbf{E} \partial \mathbf{E}'} \right|_{\mathbf{E}=\mathbf{E}'=0} \tag{2.11}$$

Polarizabilities are intricately related to excitation energies. Excitation energies are located at the poles of the polarizability tensor, and the solution to Casida's eigenvalue problem yields these excitation energies. To determine the polarizabilities from these energies, the relationship derived by Kauzmann [17] is relevant

$$\alpha(\omega) = \frac{2}{3} \sum_j \frac{(E_j - E_0) \left| \left\langle \Psi_0 \middle| \hat{\mathbf{D}} \middle| \Psi_j \right\rangle \right|^2}{(E_j - E_0)^2 - \omega^2} = \sum_j \frac{f_{0j}}{(E_j - E_0)^2 - \omega^2} \tag{2.12}$$

where the spectroscopic oscillator strengths f_{0j} are

$$f_{0j} = \frac{2}{3}(E_j - E_0) \left| \left\langle \Psi_0 \left| \hat{\mathbf{D}} \right| \Psi_j \right\rangle \right|^2 \tag{2.13}$$

with $\hat{\mathbf{D}}$ being the transition dipole moment operator and $(E_j - E_0)$ being the vertical electronic transition energy from state $0 \rightarrow j$. The spectroscopic oscillator strengths observe the Thomas-Reiche-Kuhn (TRK) rule of

$$\sum_{j \neq 0} f_{0j} = N \tag{2.14}$$

where N is the number of electrons.

2.4 Implementation

The solution to Casida's eigenvalue problem was implemented in a C++ programming language environment through heavy use of the C++ interface of the Intel Math Kernel Library (MKL). The implementation was constructed serially, however the MKL is a multi-threaded library. This allows for some small measure of parallelism to be exhibited at run time. No quadrature routines were created in this project, instead the quadrature of NWChem [18] was used to evaluate the required integrals and then fed into this implementation. Only light atoms and small diatomic or triatomic molecules were considered.

The ground state energy and wavefunction of an optimized geometry were first determined using the variational Hartree-Fock method with the overlap, kinetic, and potential energy integrals needed being evaluated in NWChem. Diagonalization of the overlap matrix was done using the symmetric eigensolver of the MKL and all matrix multiplications were accomplished using the MKL version of LAPACK's famous dgemm function. Diagonalization of the Fock matrix was accomplished using the general eigensolver of the MKL.

From there, along with molecular dipole integrals of this ground state which were also evaluated in NWChem, the transition energies and perturbed electronic density were determined according to Casida's equations. The transformation of the dipole molecular integrals from the atomic basis set to the molecular basis set was accomplished using the four quarter transformation algorithm developed by Elbert [19]. With these quantities the perturbed electronic density and transition energies were calculated. From the transition energies and perturbed density, the dynamic polarizability was found.

Chapter 3

Results

The results of solving Casida's eigenvalue problem are the square of the transition energies as the eigenvalues and the perturbed electronic density as the eigenvectors. From these quantities numerous properties of chemical significance can be derived, as shown above. To demonstrate the functionality of the TDDFT response code, the dynamic polarizability was calculated in addition to the transition energies and oscillator strengths. Here the results of such a calculation on the molecule N_2 are shared.

3.1 SCF Energy

The solutions to the TDDFT equations are sensitive to the ground state energy, as the excited state determination is only relative to the ground state [20]. For this reason, it is worth while to the examine the ground state energies obtained through an SCF procedure. The ground state energies of various small molecules were calculated using the Hartree-Fock method, with integral values being generated by the NWChem software package. Close agreement between NWChem's calculated orbital energies and the TDDFT program's orbital energies is evident with inspection. Differences between NWChem and the TDDFT response code were less than milli-Hartree in

nearly all cases. Appendix A contains the results for the other small molecules that were investigated.

Table 3.1: SCF energy of N_2

SCF Energy of N_2			
Basis: 6-31G			
Orbital	Energy (a.u.)		
	NWChem	Mine	$\|\Delta\|$
1	-15.7156	-15.7157	0.0001
2	-15.7120	-15.7121	0.0001
3	-1.5338	-1.5338	0.0000
4	-0.7721	-0.7721	0.0000
5	-0.6304	-0.6304	0.0000
6	-0.6259	-0.6259	0.0000
7	-0.6259	-0.6259	0.0000
8	0.1556	0.1556	0.0000
9	0.1556	0.1556	0.0000
10	0.5929	0.5926	0.0003
11	0.7823	0.7823	0.0000
12	0.8456	0.8455	0.0001
13	0.8456	0.8455	0.0001
14	0.9453	0.9454	0.0001
15	1.0126	1.0126	0.0000
16	1.0126	1.0126	0.0000
17	1.1667	1.1666	0.0001
18	1.5860	1.5856	0.0004

3.2 Response Theory

The following transition energies and oscillator strengths were obtained through the use of the TDDFT linear response code. These values were compared with the transition energies and oscillator strengths of NWChem's linear response module.

Table 3.2: Transition energies and oscillator strengths of N_2

Transition Energies of N_2						
Basis: 6-31G, Hfexch						
Root	Energy (a.u.)			Oscillator Strength		
	NWChem	Mine	$\|\Delta\|$	NWChem	Mine	$\|\Delta\|$
1	0.2882	0.2882	0.0000	0.0000	0.0000	0.0000
2	0.3259	0.3259	0.0000	0.0000	0.0000	0.0000
3	0.3259	0.3259	0.0000	0.0000	0.0000	0.0000
4	0.3448	0.3448	0.0000	0.0000	0.0000	0.0000
5	0.3448	0.3448	0.0000	0.0000	0.0000	0.0000
6	0.5705	0.5704	0.0000	0.2847	0.2847	0.0000
7	0.5705	0.5704	0.0000	0.2847	0.2847	0.0000
8	0.5860	0.5860	0.0000	0.8648	0.8644	0.0004
9	0.8778	0.8775	0.0003	1.3516	1.3518	0.0002
10	0.8787	0.8784	0.0003	0.0000	0.0000	0.0000
11	0.8787	0.8784	0.0003	0.0000	0.0000	0.0000
12	1.0010	1.0008	0.0002	0.0000	0.0000	0.0000
13	1.0391	1.0392	0.0000	0.0953	0.0946	0.0006
14	1.0391	1.0392	0.0000	0.0953	0.0945	0.0008
15	1.0507	1.0507	0.0000	0.0000	0.0000	0.0000

Continued on next page

Table 3.2 – continued from previous page

Root	Energy (a.u.)			Oscillator Strength		
	NWChem	Mine	$\|\Delta\|$	NWChem	Mine	$\|\Delta\|$
16	1.0532	1.0531	0.0000	0.4635	0.4643	0.0008
17	1.0532	1.0531	0.0000	0.4635	0.4642	0.0007
18	1.0534	1.0534	0.0000	0.0000	0.0000	0.0000
19	1.0534	1.0534	0.0000	0.0000	0.0000	0.0000
20	1.0717	1.0716	0.0001	0.0000	0.0000	0.0000
21	1.1371	1.1371	0.0000	0.0000	0.0000	0.0000
22	1.1371	1.1371	0.0000	0.0000	0.0000	0.0000
23	1.1765	1.1766	0.0001	0.2622	0.2621	0.0000
24	1.1765	1.1766	0.0001	0.2622	0.2621	0.0001
25	1.1791	1.1790	0.0001	0.0000	0.0000	0.0000
26	1.1810	1.1810	0.0000	0.0750	0.0751	0.0001
27	1.1984	1.1984	0.0000	0.0000	0.0000	0.0000
28	1.1984	1.1984	0.0000	0.0000	0.0000	0.0000
29	1.2242	1.2243	0.0000	0.0000	0.0000	0.0000
30	1.2252	1.2253	0.0000	0.0000	0.0000	0.0000
31	1.2252	1.2253	0.0000	0.0000	0.0000	0.0000
32	1.2591	1.2592	0.0000	0.2593	0.2590	0.0003
33	1.2989	1.2990	0.0001	0.0000	0.0000	0.0000
34	1.2989	1.2990	0.0001	0.0000	0.0000	0.0000
35	1.3110	1.3110	0.0000	0.0000	0.0000	0.0000
36	1.3276	1.3276	0.0000	0.0000	0.0000	0.0000
37	1.3276	1.3276	0.0000	0.0000	0.0000	0.0000
38	1.3923	1.3923	0.0000	0.0689	0.0690	0.0001
39	1.4143	1.4143	0.0000	0.0874	0.0874	0.0000

Continued on next page

Table 3.2 – continued from previous page

Root	Energy (a.u.)			Oscillator Strength		
	NWChem	Mine	$\|\Delta\|$	NWChem	Mine	$\|\Delta\|$
40	1.4143	1.4143	0.0000	0.0874	0.0874	0.0000
41	1.5328	1.5327	0.0001	0.0468	0.0466	0.0003
42	1.5352	1.5353	0.0000	0.0000	0.0000	0.0000
43	1.7663	1.7656	0.0006	0.0000	0.0000	0.0000
44	1.7663	1.7657	0.0006	0.0000	0.0000	0.0000
45	1.7970	1.7965	0.0005	0.0003	0.0003	0.0001
46	1.8305	1.8302	0.0003	0.2006	0.2009	0.0003
47	1.9263	1.9263	0.0000	0.0263	0.0263	0.0000
48	1.9263	1.9263	0.0000	0.0263	0.0263	0.0000
49	1.9324	1.9324	0.0000	0.0000	0.0000	0.0000
50	1.9657	1.9652	0.0005	0.0000	0.0000	0.0000
51	2.0599	2.0600	0.0001	0.0000	0.0000	0.0000
52	2.1041	2.1042	0.0000	0.0000	0.0000	0.0000
53	2.1041	2.1042	0.0000	0.0000	0.0000	0.0000
54	2.2059	2.2059	0.0000	0.2405	0.2403	0.0003
55	2.6861	2.6857	0.0004	0.1079	0.1081	0.0002
56	15.1713	15.1714	0.0001	0.1903	0.1903	0.0000
57	15.1713	15.1714	0.0001	0.1903	0.1903	0.0000
58	15.1725	15.1726	0.0001	0.0000	0.0000	0.0000
59	15.1725	15.1726	0.0001	0.0000	0.0000	0.0000
60	15.8372	15.8370	0.0002	0.0000	0.0000	0.0000
61	15.8399	15.8398	0.0001	0.0506	0.0505	0.0001
62	15.9238	15.9238	0.0000	0.1866	0.1867	0.0001
63	15.9286	15.9287	0.0001	0.0000	0.0000	0.0000

Continued on next page

Table 3.2 – continued from previous page

Root	Energy (a.u.)			Oscillator Strength		
	NWChem	Mine	$\|\Delta\|$	NWChem	Mine	$\|\Delta\|$
64	15.9380	15.9380	0.0000	0.0000	0.0000	0.0000
65	15.9380	15.9380	0.0000	0.0000	0.0000	0.0000
66	15.9405	15.9406	0.0001	0.1187	0.1187	0.0000
67	15.9405	15.9406	0.0001	0.1187	0.1187	0.0000
68	16.0596	16.0597	0.0001	0.0057	0.0057	0.0000
69	16.0626	16.0627	0.0001	0.0000	0.0000	0.0000
70	16.3035	16.3035	0.0000	0.0086	0.0086	0.0000
71	16.3035	16.3035	0.0000	0.0086	0.0086	0.0000
72	16.3050	16.3051	0.0001	0.0000	0.0000	0.0000
73	16.3050	16.3051	0.0001	0.0000	0.0000	0.0000
74	16.3425	16.3426	0.0001	0.0000	0.0000	0.0000
75	16.3426	16.3427	0.0001	0.0240	0.0241	0.0000
76	16.7553	16.7548	0.0005	0.0000	0.0000	0.0000
77	16.7585	16.7582	0.0003	0.0091	0.0091	0.0000

The differences between NWChem's transition energies and the TDDFT linear response code's transition energies are negligible in most cases, with differences on the order of 10's of micro-Hartrees. The oscillator strengths also showed close agreement between NWChem's calculated value and the TDDFT linear response code's calculated value. The differences were once again of the order of 10^{-5}. The remaining small molecule's data is presented in the Appendix. Using these transition energies and oscillator strengths, a theoretical excitation spectra can be constructed

with a simple plot of frequency versus transition strength. A plot of this is presented here.

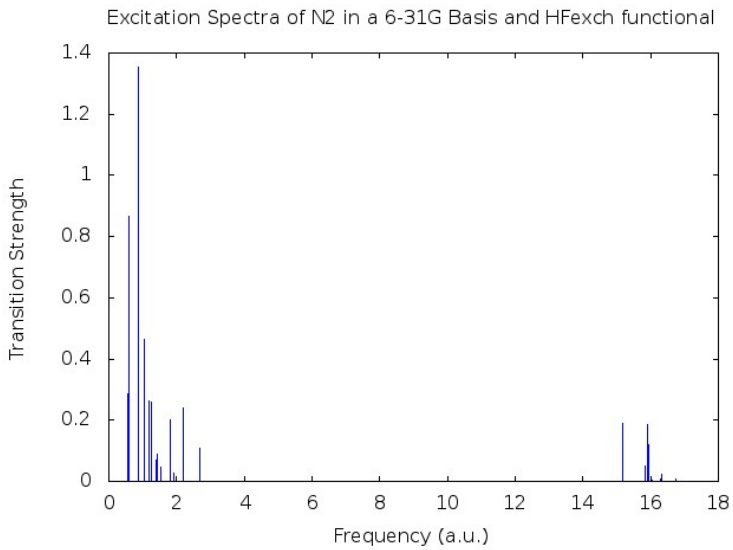

Figure 3.1: Calculated excitation spectra of N_2.

Also from the above transition energies and oscillator strengths, the frequency dependent polarizability can be calculated according to equation (2.12). The polarizability calculated here is for an infinite lifetime excitation. In order to simulate a finite lifetime, in each excitation, an energy-broadening term unique to that transition must be included [21]. Plotting the polarizability as a function of frequency of radiation gives the following plot.

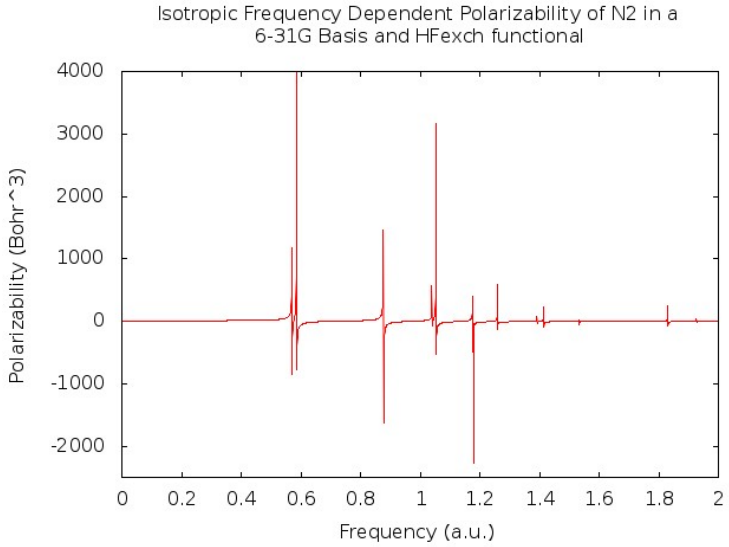

Figure 3.2: Calculated polarizability of N_2.

The large increase in polarizability at 0.570 a.u. corresponds to the lowest level electronic excitation. This excitation energy is in fair agreement with Koopmans' theorem [22], which states that the first ionization energy of a molecule can be approximated as the energy of the highest occupied molecular orbital. Of course, inspection of the polarizability relation of equation (2.12) also shows that polarizability will have poles at the excitation energies.

Chapter 4

Parallelization of the Orbital Localization Algorithm

The barrier to applying correlated *ab initio* methods to large molecular systems is tied to the prohibitive scaling costs of these methods [23]. Some of this cost can be alleviated by applying an orbital localization algorithm to the occupied orbitals. This reduces the space that the orbitals span, hence reducing the *inter*-orbital correlation and making the *intra*-orbital correlation the leading correctional term [24]. The goal of all localization algorithms is to apply a series of unitary transformations to an occupied orbital until that orbital satisfies the given criteria for localization. This can be done because single determinant wavefunctions are invariant to unitary transformations among their occupied orbitals. The details of three widely used algorithms [25] are presented here, as well as the one-sided Jacobi algorithm on which the localization algorithms are based, followed by a modern description of the implementation of these algorithms.

4.1 Algorithms

4.1.1 The One-Sided Jacobi Algorithm

The one-sided Jacobi algorithm takes an $m \times n$ matrix A and generates a matrix V such that

$$AV = H \tag{4.1}$$

where the columns of matrix H are orthogonal. The matrix H is generated through consecutive plane rotations of pairs of columns of the matrix A. Each rotation will have the form

$$\begin{pmatrix} a_i & a_j \end{pmatrix} \begin{pmatrix} c & -s \\ s & c \end{pmatrix} = \begin{pmatrix} a'_i & a'_j \end{pmatrix} \tag{4.2}$$

where a_i and a_j are columns of matrix A with $i \neq j$ and $c = \cos(\theta)$ and $s = \sin(\theta)$. The matrix $\begin{pmatrix} c & -s \\ s & c \end{pmatrix}$ is the rotation matrix, of which there are $\frac{n(n-1)}{2}$ unique pairs of columns that can be done for a matrix with length n. Completing all $\frac{n(n-1)}{2}$ unique rotations is known as completing a sweep. Sweeps are performed until all the columns of the matrix are orthogonal throughout a single sweep, within some convergence criterion. Assuming a reasonable selection of the rotation angles, the convergence of this algorithm is quadratic [26].

The selection of this angle α has been algebraically determined in the literature [27], and has values

$$sin(4\alpha) = \frac{B_{st}}{(A_{st}^2 + B_{st}^2)^{(1/2)}} \tag{4.3}$$

$$cos(4\alpha) = \frac{-A_{st}}{(A_{st}^2 + B_{st}^2)^{(1/2)}} \tag{4.4}$$

$$0 \leq \alpha \leq \frac{\pi}{2}. \tag{4.5}$$

The restriction on α is to keep the rotation angle between 0 and 2π. The general forms of A_{st} and B_{st} are

$$A_{st} = \langle st\,|\Omega|\,st\rangle - \frac{1}{4}\left[\langle ss\,|\Omega|\,ss\rangle + \langle tt\,|\Omega|\,tt\rangle - 2\,\langle ss\,|\Omega|\,tt\rangle\right] \tag{4.6}$$

$$B_{st} = \langle ss\,|\Omega|\,st\rangle - \langle tt\,|\Omega|\,st\rangle \tag{4.7}$$

The functional Ω is algorithm specific, and defined in the appropriate sections below. The proper selection of α will determine if the functional Ω that generated the vectors a_i and a_j is to be maximized or minimized, also algorithm specific . Letting the rotation angle θ be

$$\theta = \alpha + \frac{k\pi}{2} \tag{4.8}$$

will maximize Ω and

$$\theta = \alpha + \frac{(2k+1)\pi}{4} \tag{4.9}$$

will minimize Ω for arbitrary integer k.

4.1.2 Foster and Boys

Boys [28] algorithm was chronologically the first of the three methods to be conceived. The Boys algorithm minimizes the spatial extent of the molecular orbitals, hence concentrating the orbital density into a local area about atomic centers. The only additional required information for the algorithm not already obtained from a ground-state theory are the dipole integrals. The algorithm scales as N^3, where N is a scaling factor related to either the number of electrons or basis functions, but the resulting orbitals are less local [25]. This algorithm does not separate σ and π bonds, but instead produces two τ or "banana orbitals" [29], which are similar in shape to $\sigma + \pi$ and $\sigma - \pi$. The localization criteria is summarized as

$$B\{\varphi_i\} = \sum_{i=1}^{N} \left\langle ii\,\left|\Omega^B\right|\,ii\right\rangle \tag{4.10}$$

where

$$\Omega^B(\mathbf{r_1}, \mathbf{r_2}) = (\mathbf{r_1} - \mathbf{r_2})^2 \tag{4.11}$$

4.1.3 Edmiston and Ruedenberg

Edmiston and Ruedenberg created an algorithm that localizes molecular orbitals by maximizing the self-repulsion energy [24]. The algorithm scales as N^5, due to the fact that it requires two electron integrals in the molecular orbital basis. This means that the atomic integrals must be transformed, a procedure that scales as N^5. The σ and π bond characteristics are kept separate. The localization criteria is summarized as

$$ER\{\varphi_i\} = \sum_{i=1}^{N} \left\langle ii \left| \Omega^{ER} \right| ii \right\rangle \tag{4.12}$$

where

$$\Omega^{ER}(\mathbf{r_1}, \mathbf{r_2}) = |\mathbf{r_1} - \mathbf{r_2}|^2 \tag{4.13}$$

4.1.4 Pipek and Mezey

The Pipek-Mezey algorithm localizes molecular orbitals by maximizing the sum of squares of the Mulliken charges on atomic centers [29]. This algorithm scales as N^3, with only knowledge of the overlap matrix and dipole integrals required. This algorithm does maintain separate σ and π bonds. The localization criteria is summarized as

$$D = \sum_{i=1}^{N} \sum_{A} (Q_{ii}^A)^2 \tag{4.14}$$

with

$$Q_{ii}^{A} = \sum_{\mu \in A} \langle i \,|P_{\mu}|\, i \rangle \tag{4.15}$$

where Q_{ii}^{A} is the gross atomic Mulliken populations of the orbital $|i\rangle$ and the projection operator P_{μ}^{M} projects out atomic basis function μ according to

$$P_{\mu}^{M} = \frac{1}{2}(|\bar{\mu}\rangle\langle\mu| + |\mu\rangle\langle\bar{\mu}|) \tag{4.16}$$

and finally

$$|\bar{\mu}\rangle = \sum_{v} (S^{-1})_{v\mu} \,|v\rangle \tag{4.17}$$

with S being the overlap matrix used in the ground state theory to generate the molecular orbitals.

4.2 Parallelization

One efficient implementation of these one-sided Jacobi like algorithms on a distributed memory machine involves the use of systolic arrays in order to minimize communication costs and maximize performance through parallelization. A basic systolic array can be thought of as a linear array of processors, each with its own memory, that communicate by passing information to their nearest neighbor. Communication can occur with either the left or right neighbor or even both, as needed. The communication pattern is entirely algorithm dependent. For the implementation of these localization algorithms, a bi-directional communication pattern is useful. Consider a single sweep of one of the above algorithms in which there are six orbitals (i.e.. six columns in the matrix) to be localized on a machine with three processors dedicated to this task. The orbitals are distributed evenly pairwise over the processors, as illustrated in Figure 4.1.

The algorithm will commence with each processor performing its part of the current sweep with the two orbitals it currently possesses. Once finished with the first step,

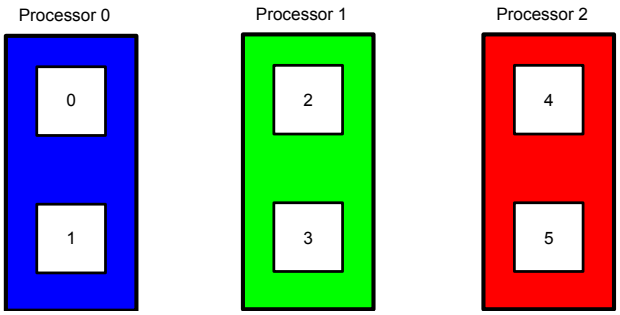

Figure 4.1: Initial distrubtion of matrix columns among processors.

the processors will interchange their orbitals according to the communication pattern in Figure 4.2. This communication pattern will continue until all the pairings of the

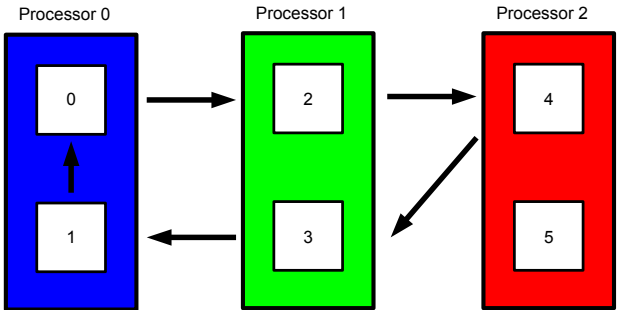

Figure 4.2: Communication pattern after first pair of orbitals have had the algorithm applied.

sweep have been realized. For a matrix with n columns, there are $\frac{1}{2}(n-1)$ rotations to be done per sweep. As outlined by Zhou [30], a full sweep can be accomplished with $(n-1)$ steps with this communication pattern. After $(n-1)$ steps, the orbitals will be back in their original positions and can easily be checked for convergence. To

accomplish this type of communication, the Message Passing Interface (MPI) API is ideally suited. Using MPI, the orbitals themselves can be passed among processors at each step with minimal communication cost. Each orbital is sent directly from one processor to its destination by specifying a few parameters such as destination ID, the type and number of elements to be sent, and the message handle. Another method of parallelization involves the use of the OpenMP API. OpenMP requires only a set of directives to be specified by the user, and then creates an internal list of commands that will handle all communication and parallelization.

The one sided Jacobi algorithm lends itself well to parallelization, as opposed to the two sided Jacobi algorithm. The rotations of the one sided Jacobi algorithm only affect two columns, leaving the rest unchanged. This allows for the columns to be distributed across a machine without penalty. The two sided Jacobi algorithm affects pairs of both rows and columns. To see this, take note that the two sided Jacobi algorithm completes a rotation of matrix A by doing the multiplication of

$$RAR^T = A' \tag{4.18}$$

where R is the identity with a sub-matrix of the same rotation matrix as in the one sided Jacobi, and R^T is its transpose. It is this transpose that causes the rows of the matrix to be linked in such a way as to render the simple column distribution inapplicable. That is not to say that the two sided Jacobi algorithm cannot be parallelized, but rather that the simple distribution is not usable. Instead of distributing the columns pairwise across a machine, the algorithm calls for a block distribution to be used along with a complicated communication pattern for updating the

As a first step towards the creation of a working localization code, a symmetric Jacobi eigensolver was created in a C++ coding environment following the algorithm developed by Sameh [31]. In this algorithm, a number of different rotations of a sweep were combined into a single rotation matrix. The rotations were then applied

simultaneously using the parallel directive of the OpenMP API around a matrix matrix multiplication routine. Unfortunately the created code suffered from rotations that combined in unexpected ways to effectively undo each other. This occurrence prevented the algorithm from converging to a diagonal matrix with the eigenvalues of the starting matrix as its entries. The following is a performance graph of FLOPS (floating point operations per second) versus length of initial square matrix of a *serial* Jacobi eigenvalue algorithm.

As is easily seen, there is a quickly reached performance maximum for a serial

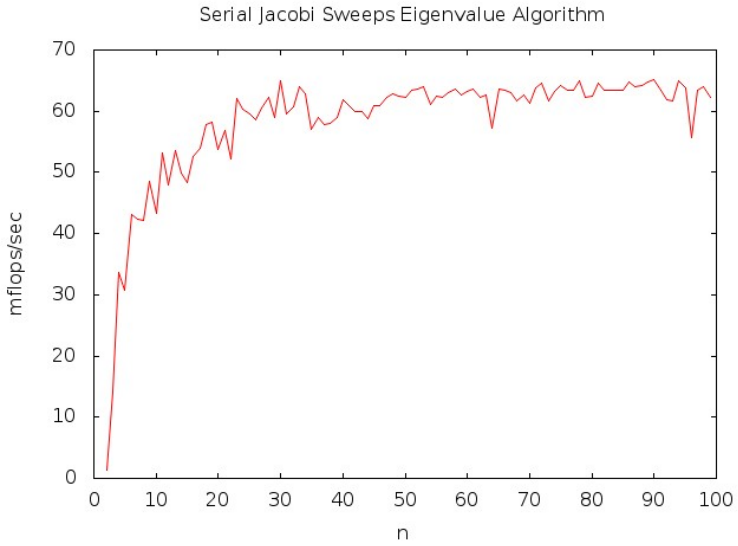

Figure 4.3: Performance graph of a serial Jacobi eigenvalue algorithm

algorithm. To demonstrate accuracy a graph of the residue of the algorithm is now presented. The reside is calculated as the two norm of the matrix of the result of $(A - \lambda * I) * V$ where A is the matrix, λ are the eigenvalues, I is the identity matrix, and V are the eigenvectors. This value should analytically be zero, and numerically within a tolerance of zero. The answer could also be compared to a known answer

from an established API, such as LAPACK [32].

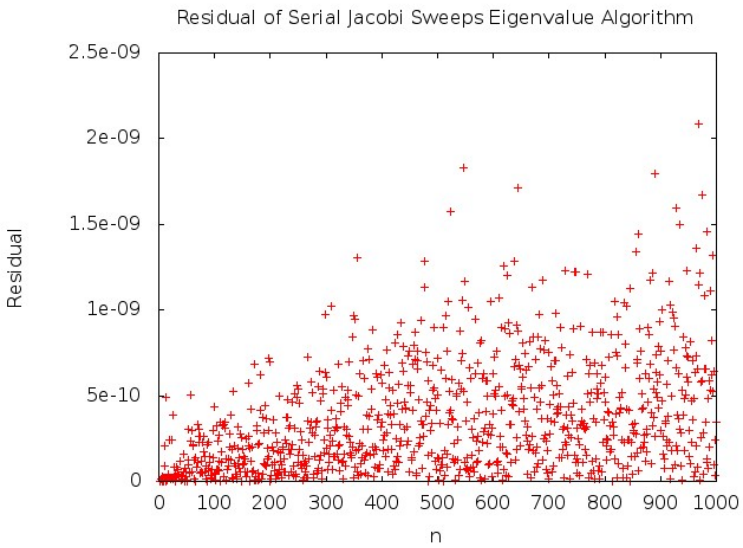

Figure 4.4: Residue graph of a serial Jacobi eigenvalue algorithm

With a correctly implemented parallel Jacobi algorithm, the maximum performance will be greatly raised while maintaining the same level of accuracy. As is demonstrated by the following graphs, the current implementation of the parallel code leaves much to be desired. An as of yet undiscovered bug is thought to be the cause.

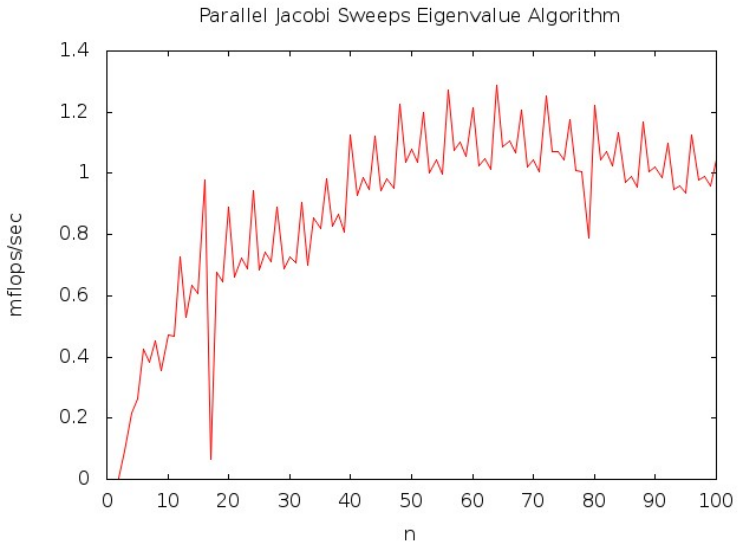

Figure 4.5: Performance graph of a parallel Jacobi eigenvalue algorithm

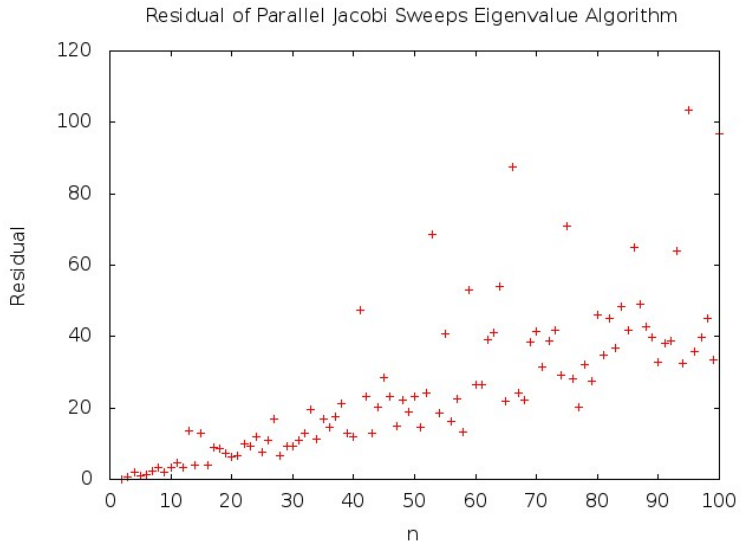

Figure 4.6: Residue graph of a parallel Jacobi eigenvalue algorithm

Currently, the simultaneous multiple rotations scheme seems to cause many rotations to effectively undo each other, leading to lots of wasted computed time (which affects performance) and keeping the system from converging (which affects accuracy). Thus both metrics of import are impacted negatively in this parallel implementation. The following performance and residue graphs echo these sentiments.

Conclusion

In this text the validity of the TDDFT equations was shown through the one-to-one correspondence between an external potential and an electronic current density and the one-to-one correspondence between the same electronic current density and the electronic density. Then the origin of the time-dependent Kohn-Sham equations was discussed. The linear response formalism was then explored and the quintessential equation (1.25) derived. The final transformation was that of Casida's matrix formulation and subsequent casting of a psuedo-eigenvalue problem into the form presented by equation (1.55). This eigenvalue problem is the working form implemented in the TDDFT-LR code created here.

The generality of the machinery developed in the creation of a TDDFT-LR code was demonstrated here. The ability to describe chemically important concepts as the second derivative of the energy with respect to some perturbation allows for the evaluation of these properties within the linear response framework. Some specific examples were demonstrated, including the NMR shielding tensor and the dynamic polarizability. The implementation of the above mentioned machinery was then detailed.

The results of the TDDFT-LR code when applied to a small diatomic molecule were explored. The agreement between the large software package NWChem and the TDDFT-LR code was established. The resulting excitation spectra and polarizability plots were displayed.

The separate but related problem of orbital localization was discussed. The

motivation for such an algorithm was developed. The Jacobi plane rotation algorithm, on which the three most used orbital localization methods are based on, was explored. The three localization algorithms were then displayed, followed by comments on an the parallelization of these algorithms.

With the final goal of calculating forces on excited states firmly fixed, the path forward includes creating an algorithm to take the derivatives of the excited states calculated from the linear response time-dependent density-functional theory. Using these derivatives, the potential energy surfaces can be constructed and the excited state geometry can be optimized. Then excited state properties can be calculated with an accurate excited state wavefunction. These next steps must also be translated into the numerical environment of MADNESS [33], making use of the accuracy and parallelism provided in the MADNESS framework.

Bibliography

[1] Szabo and Ostlund. *Modern Quantum Chemistry: Introduction to Advanced Electronic Structure Theory*. Dover, 1996.

[2] P. Hohenberg and W. Kohn. Inhomogeneous electron gas. *Phys. Rev.*, 136, 1964.

[3] C. Møller and M. S. Plesset. *Phys. Rev.*, 46(618), 1934.

[4] P Carsky. *Encyclopedia of Computational Chemistry*, page 615. Wiley, 1998.

[5] R. J. Bartlett, editor. *Modern Ideas in Coupled-Cluster Methods*. World Scientific, 1997.

[6] Ira Levine. *Quantum Chemistry*. Pearson Prentice Hall, 6 edition, 2009.

[7] Erich Runge and E. K. U. Gross. Density-functional theory for time-dependent systems. *Physical Review Letters*, 52(12), 1984.

[8] R. van Leeuwen. Mapping from densities to potentials in time-dependent density-functional theory. *Phys. Rev. Lett.*, 82:3863, 1999.

[9] Nogueira Rubio Burke Gross Marques, Ullrich, editor. *Time-Dependent Density Functional Theory*. Lecture Notes in Physics. Springer, 2006.

[10] Petersilka M., U. J. Grossman, and E. K. U. Gross. Excitation energies from time-dependent density-functional theory. *Physical Review Letters*, 1996.

[11] E. K. U. Gross, J. F. Dobson, and Petersilka M. Density functional theory of time-dependent phenomena. *Topics in Chemistry*, 181(81), 1996.

[12] M. E. Casida. Time-dependent density functional response theory for molecules. In D. E. Chong, editor, *Recent Advances in Density Functional Methods*. World Scientific, 1995.

[13] A. L. Fetter and J. D. Walecka. *Quantum Theory of Many-Particle Systems*. McGraw-Hill: New York, 1971.

[14] Jochen Autschbach and Tom Ziegler. Double perturbation theory: A powerful tool in computational coordination chemistry. *Coord. Chem. Rev.*, 238/239:83–126, 2003.

[15] H. Hellmann. *Z. Phys.*, 85(180), 1933.

[16] A. Willetts, J. E. Rice, D. M. Burland, and D. P. Shelton. *J. Chem. Phys.*, 97, 1992.

[17] W. Kauzmann. *Quantum Chemistry.* Academic Press, New York, 1957.

[18] M. Valiev, E.J. Bylaska, N. Govind, K. Kowalski, T.P. Straatsma, H.J.J. van Dam, D. Wang, J. Neiplocha, E. Apra, T. L. Windus, and W. A. de Jong. Nwchem: a comprehensive and scalable open-source solution for large scale molecular simulations. *Comput. Phys. Commun.*, 181, 2010.

[19] S. T. Elbert. Numerical algorithms in chemistry: Algebraic methods, 1978.

[20] Andreas Dreuw and Martin Head-Gordon. Single-reference ab initio methods for the calculation of excited states of large molecules. *Chem. Rev.*, pages 4009–4037, 2005.

[21] J. Autschbach L. Jensen and G. C. Schatz. Finite lifetime effects on the polarizability within time-dependent density-functional theory. *J. Chem. Phys.*, 122, 2005.

[22] Tjalling Koopmans. Über die zuordnung von wellenfunktionen und eigenwerten zu den einzelnen elektronen eines atoms. *Physica*, 1934.

[23] John M. Millam and Gustavo E. Scuseria. Linear scaling conjugate gradient density matrix search as an alternative to diagonalization for first principles electronic structure calculations. *J. Chem. Phys.*, 106, 1997.

[24] C. Edmiston and K. Ruedenberg. *Rev. Mod. Phys.*, 35(457), 1963.

[25] Ida-Marie Høvik, Branislav Jansik, and Poul Jørgensen. Pipek-mezey localization of occupied and virtual orbitals. *Journal of Computational Chemistry*, 34:1456–1462, 2013.

[26] B. B. Zhou, R. P. Brent, and M. Kahn. A one-sided jacobi algorithm for the symmetrid eigenvalue problem. *IEEE 1st International Conference on Algorithms and Architectures for Parallel Processing*, 1995.

[27] R. Barr and H. Basch. *Chem. Phys. Lett.*, 32(537), 1975.

[28] S. F. Boys. *Rev. Mod. Phys*, 32(296), 1960.

[29] J. Pipek and P. G. Mezey. *J. Chem. Phys.*, 90(4916), 1989.

[30] B. B. Zhou and R. P. Brent. On parallel implementation of the one-sided jacobi algorithm for singular value decompositions. *Journal of Parallel and Distributed Computing*, 1997.

[31] Ahmed H. Sameh. On jacobi and jacobi-like algorithms for a parallel computer. *Mathematics of Computation*, 25(115), 1971.

[32] E. Anderson, Z. Bai, C. Bischof, S. Blackford, J. Demmel, J. Dongarra, J. Du Croz, A. Greenbaum, S. Hammarling, A. McKenney, and D. Sorensen. *LAPACK Users' Guide*. Society for Industrial and Applied Mathematics, Piladelphia, Pa, third edition, 1999.

[33] R. J. Harrison, G. I. Fann, Z. Gan Yanai, and G. Beylkin. *J. Chem. Phys.*, 121, 2005.

Appendix

Appendix

A SCF Energies

The remaining data of ground state energies from from all of the small molecules investigated are presented here.

Table A.1: SCF energy of He

SCF Energy of He			
Basis: aug-cc-pVDZ			
Orbital	Energy (a.u.)		
	NWChem	Mine	$\|\Delta\|$
1	-0.9171	-0.9170	0.0001
2	0.1744	0.1744	0.0000
3	0.5304	0.5305	0.0001
4	0.5304	0.5305	0.0001
5	0.5304	0.5305	0.0001
6	1.7135	1.7137	0.0002
7	3.0249	3.0251	0.0002
8	3.0249	3.0251	0.0002
9	3.0249	3.0251	0.0002

Table A.2: SCF energy of H_2

SCF Energy of H_2			
Basis: 6-31++G**			
Orbital	Energy (a.u.)		
	NWChem	Mine	$\|\Delta\|$
1	-0.5978	-0.5978	0.0000
2	0.0751	0.0752	0.0001
3	0.0884	0.0884	0.0000
4	0.3071	0.3072	0.0001
5	0.9363	0.9363	0.0000
6	1.3908	1.3908	0.0000
7	1.9577	1.9577	0.0000
8	1.9577	1.9577	0.0000
9	2.7366	2.7366	0.0000
10	2.9378	2.9378	0.0000
11	2.9378	2.9378	0.0000
12	4.5737	4.5737	0.0000

Table A.3: SCF energy of H_2O

SCF Energy of H_2O			
Basis: 6-31+G*			
Orbital	Energy (a.u.)		
	NWChem	Mine	$\|\Delta\|$
1	-20.5782	-20.5765	0.0017
2	-1.3609	-1.3604	0.0005
3	-0.7318	-0.7314	0.0004
4	-0.5828	-0.5823	0.0005
5	-0.5094	-0.5089	0.0005
6	0.1466	0.1467	0.0001
7	0.2190	0.2191	0.0001
8	0.2508	0.2509	0.0001
9	0.2525	0.2526	0.0001
10	0.3595	0.3597	0.0001
11	0.3876	0.3877	0.0001
12	1.2478	1.2480	0.0002
13	1.3477	1.3479	0.0002
14	1.3898	1.3903	0.0005
15	1.4046	1.4051	0.0005
16	1.4089	1.4093	0.0004
17	1.4737	1.4740	0.0003
18	2.0099	2.0104	0.0005
19	2.0148	2.0152	0.0004
20	2.0541	2.0546	0.0005
21	2.6365	2.6369	0.0004
22	3.0386	3.0390	0.0004
23	4.1078	4.1084	0.0006

B Transition Energies and Oscillator Strengths

Here the tables of transition energies and oscillator strengths of the remaining investigated small molecules are presented.

Table B.1: Transition energies and oscillator strengths of He

Transition Energies of He						
Basis: aug-cc-pVDZ, Hfexch						
Root	Energy (a.u.)			Oscillator Strength		
	NWChem	Mine	$\lvert\Delta\rvert$	NWChem	Mine	$\lvert\Delta\rvert$
1	0.8221	0.8219	0.0002	0.0000	0.0000	0.0000
2	1.0325	1.0324	0.0001	0.4414	0.4411	0.0003
3	1.0325	1.0324	0.0001	0.4414	0.4411	0.0003
4	1.0325	1.0324	0.0001	0.4414	0.4411	0.0003
5	2.1944	2.1944	0.0000	0.0000	0.0000	0.0000
6	3.3234	3.3235	0.0001	0.2279	0.2281	0.0002
7	3.3234	3.3235	0.0001	0.2279	0.2281	0.0002
8	3.3234	3.3235	0.0001	0.2279	0.2281	0.0002

Table B.2: Transition energies and oscillator strengths of H_2

Transition Energies of H_2						
Basis: 6-31++G**, Hfexch						
Root	Energy (a.u.)			Oscillator Strength		
	NWChem	Mine	$\|\Delta\|$	NWChem	Mine	$\|\Delta\|$
1	0.4709	0.4709	0.0000	0.2927	0.2927	0.0000
2	0.4919	0.4919	0.0000	0.0000	0.0000	0.0000
3	0.6453	0.6453	0.0000	0.3536	0.3536	0.0000
4	1.2080	1.2080	0.0000	0.0000	0.0000	0.0000
5	1.5956	1.5956	0.0000	0.0434	0.0434	0.0000
6	2.0981	2.0979	0.0002	0.8283	0.8286	0.0003
7	2.0981	2.0984	0.0002	0.8283	0.8281	0.0003
8	2.8117	2.8117	0.0000	0.0000	0.0000	0.0000
9	2.9967	2.9584	0.0383	0.0000	0.0000	0.0000
10	2.9967	3.0350	0.0383	0.0000	0.0000	0.0000
11	4.5882	4.5882	0.0000	0.0052	0.0052	0.0000

Table B.3: Transition energies and oscillator strengths of H_2O

Transition Energies of H_2O						
Basis: 6-31+G*, Hfexch						
Root	Energy (a.u.)			Oscillator Strength		
	NWChem	Mine	$\|\Delta\|$	NWChem	Mine	$\|\Delta\|$
1	0.3440	0.3436	0.0004	0.0661	0.0661	0.0000
2	0.4211	0.4207	0.0004	0.0000	0.0000	0.0000
3	0.4312	0.4308	0.0004	0.1311	0.1310	0.0001
4	0.4837	0.4832	0.0005	0.0273	0.0272	0.0000
5	0.5015	0.5010	0.0005	0.0039	0.0039	0.0000
6	0.5086	0.5082	0.0004	0.0388	0.0387	0.0001
7	0.5326	0.5321	0.0004	0.0000	0.0000	0.0000
8	0.5514	0.5510	0.0005	0.0010	0.0010	0.0000
9	0.5676	0.5673	0.0003	0.1718	0.1716	0.0002
10	0.5744	0.5730	0.0014	0.0422	0.0421	0.0001
11	0.5815	0.5811	0.0004	0.1500	0.1499	0.0000
12	0.6285	0.6281	0.0004	0.2355	0.2356	0.0001
13	0.6560	0.6556	0.0004	0.0013	0.0013	0.0000
14	0.7050	0.7047	0.0004	0.0000	0.0000	0.0000
15	0.7190	0.7186	0.0004	0.0021	0.0020	0.0000
16	0.7198	0.7194	0.0004	0.0304	0.0304	0.0000
17	0.7979	0.7976	0.0003	0.3113	0.3113	0.0000
18	0.8163	0.8159	0.0004	0.3632	0.3632	0.0001
19	1.2067	1.2063	0.0004	0.0168	0.0168	0.0000
20	1.2870	1.2868	0.0002	0.0000	0.0213	0.0213
21	1.2872	1.2868	0.0004	0.0214	0.0000	0.0214
22	1.3350	1.3345	0.0005	0.0292	0.0292	0.0000

Continued on next page

Table B.3 – continued from previous page

Root	Energy (a.u.)			Oscillator Strength		
	NWChem	Mine	$\|\Delta\|$	NWChem	Mine	$\|\Delta\|$
23	1.3465	1.3460	0.0005	0.0075	0.0074	0.0000
24	1.3594	1.3593	0.0001	0.0276	0.0277	0.0001
25	1.3854	1.3852	0.0002	0.0000	0.0000	0.0000
26	1.3859	1.3855	0.0004	0.0011	0.0011	0.0000
27	1.3990	1.3988	0.0002	0.0001	0.0001	0.0000
28	1.4080	1.4078	0.0002	0.0001	0.0001	0.0000
29	1.4279	1.4275	0.0004	0.0068	0.0067	0.0000
30	1.4583	1.4581	0.0003	0.0026	0.0023	0.0002
31	1.4631	1.4630	0.0002	0.0155	0.0157	0.0003
32	1.4795	1.4792	0.0002	0.1449	0.1449	0.0000
33	1.5087	1.5085	0.0002	0.0028	0.0029	0.0001
34	1.5319	1.5317	0.0002	0.0323	0.0322	0.0001
35	1.5480	1.5477	0.0003	0.3254	0.3254	0.0001
36	1.6029	1.6029	0.0001	0.0000	0.0000	0.0000
37	1.6072	1.6070	0.0002	0.1068	0.1068	0.0000
38	1.6223	1.6222	0.0002	0.0430	0.0431	0.0001
39	1.6318	1.6319	0.0000	0.0000	0.0000	0.0000
40	1.7054	1.7052	0.0002	0.1911	0.1913	0.0002
41	1.7834	1.7833	0.0001	0.0033	0.0032	0.0000
42	1.8908	1.8907	0.0000	0.0239	0.0239	0.0000
43	1.9565	1.9565	0.0000	0.0639	0.0639	0.0000
44	2.0027	2.0026	0.0000	0.0123	0.0123	0.0000
45	2.0304	2.0304	0.0000	0.0000	0.0000	0.0000
46	2.0418	2.0418	0.0001	0.7001	0.7003	0.0003

Continued on next page

Table B.3 – continued from previous page

Root	Energy (a.u.)			Oscillator Strength		
	NWChem	Mine	$\|\Delta\|$	NWChem	Mine	$\|\Delta\|$
47	2.1191	2.1191	0.0000	0.2020	0.2022	0.0003
48	2.1505	2.1502	0.0002	0.2077	0.0275	0.1802
49	2.2064	2.2064	0.0001	1.6516	1.6512	0.0004
50	2.2237	2.2236	0.0000	0.5049	0.5037	0.0012
51	2.2304	2.2303	0.0001	0.4573	0.4565	0.0009
52	2.2396	2.2397	0.0001	0.0000	0.0000	0.0000
53	2.2710	2.2709	0.0001	0.2471	0.2476	0.0004
54	2.2720	2.2719	0.0001	0.0835	0.0844	0.0009
55	2.3069	2.3065	0.0004	0.0004	0.0004	0.0000
56	2.3246	2.3246	0.0000	0.8061	0.8064	0.0003
57	2.4161	2.4158	0.0003	0.0104	0.0104	0.0000
58	2.6918	2.6917	0.0001	0.5987	0.5990	0.0003
59	2.6972	2.6970	0.0001	0.0010	0.0010	0.0000
60	2.8316	2.8315	0.0001	0.0000	0.0000	0.0000
61	2.8359	2.8358	0.0001	0.0540	0.0541	0.0001
62	2.8754	2.8754	0.0000	0.0582	0.0582	0.0000
63	2.8772	2.8772	0.0001	0.0928	0.0929	0.0001
64	3.0082	3.0080	0.0002	0.0000	0.0000	0.0000
65	3.1391	3.1389	0.0001	0.1089	0.1089	0.0000
66	3.2775	3.2775	0.0000	0.0556	0.0556	0.0000
67	3.4658	3.4657	0.0002	0.0045	0.0045	0.0000
68	3.8628	3.8627	0.0002	0.0012	0.0012	0.0000
69	4.0239	4.0240	0.0001	0.0001	0.0001	0.0000
70	4.1179	4.1180	0.0001	0.0018	0.0018	0.0000

Continued on next page

Table B.3 – continued from previous page

Root	Energy (a.u.)			Oscillator Strength		
	NWChem	Mine	$\|\Delta\|$	NWChem	Mine	$\|\Delta\|$
71	4.2844	4.2846	0.0002	0.0011	0.0011	0.0000
72	4.9210	4.9210	0.0000	0.0012	0.0012	0.0000
73	20.2781	20.2766	0.0015	0.0382	0.0381	0.0000
74	20.3042	20.3028	0.0014	0.0732	0.0732	0.0000
75	20.4587	20.4570	0.0017	0.0344	0.0344	0.0000
76	20.4835	20.4819	0.0016	0.0167	0.0167	0.0000
77	20.5740	20.5723	0.0017	0.0009	0.0009	0.0000
78	20.5978	20.5962	0.0016	0.0035	0.0035	0.0000
79	21.1272	21.1258	0.0014	0.0695	0.0695	0.0000
80	21.1693	21.1680	0.0013	0.0847	0.0847	0.0000
81	21.1700	21.1686	0.0014	0.0757	0.0757	0.0000
82	21.3410	21.3396	0.0014	0.0039	0.0039	0.0000
83	21.3907	21.3892	0.0015	0.0011	0.0011	0.0000
84	21.4787	21.4773	0.0014	0.0004	0.0004	0.0000
85	21.8316	21.8304	0.0012	0.0001	0.0000	0.0000
86	21.8327	21.8315	0.0012	0.0000	0.0000	0.0000
87	21.8727	21.8715	0.0012	0.0000	0.0000	0.0000
88	22.5279	22.5266	0.0013	0.0000	0.0000	0.0000
89	22.9182	22.9169	0.0013	0.0000	0.0000	0.0000
90	23.8086	23.8074	0.0012	0.0002	0.0002	0.0000

Vita

Bryan Sundahl was born in Austin, Texas to the loving parents of Brad and Virginia Sundahl. Bryan has two younger siblings: Erik and Amy. Bryan attended Manchaca Elementary School, then moved on to Bailey Middle School and he ended his public education at James Bowie High School in Austin, Texas. After graduation he moved on to the University of Texas at Austin, where he enrolled as a Chemistry major. After taking a large number of Mathematics courses as electives he decided to add this subject as a second major. In December of 2009 Bryan graduated with a Bachelors of Science in Chemistry and a Bachelors of Science in Mathematics. After a brief stint in public education, Bryan moved on to post-graduate work in Chemistry at the University of Tennessee, Knoxville.